Int J Clin Exp Pathol 2022;15(8):301-315
www.ijcep.com /ISSN:1936-2625/IJCEP0142257

Original Article

A novel pyroptosis-related gene signature for predicting laryngeal carcinoma prognosis

Haopeng Zhang[1], Lihua Wang[1], Ziming Yin[2], Lin Ji[1], Yu Guo[1]

[1]*Department of Otolaryngology, Shanghai Municipal Hospital of Traditional Chinese Medicine, Shanghai University of Traditional Chinese Medicine, Shanghai, China;* [2]*School of Health Science and Engineering, University of Shanghai for Science and Technology, Shanghai, China*

Received February 9, 2022; Accepted May 9, 2022; Epub August 15, 2022; Published August 30, 2022

Abstract: Pyroptosis, a newly-defined mode of cell death related to inflammation, is closely related to cancers but has not yet been studied in laryngeal carcinoma (LC). We investigated pyroptosis in LC and constructed a prognostic model. Using RNA sequencing data, we identified differentially expressed genes (DEGs) in LC and normal tissues to construct a prognostic risk model. The model's accuracy and independent prognostic value were evaluated using survival- and receiver operating characteristic (ROC)- curves; and univariate and multivariate Cox regression analyses, respectively. Gene Expression Omnibus (GEO) data was utilized as a model validation set. Differential analysis revealed 37 DEGs, and consistent clustering showed that pyroptosis-related genes could predict LC prognosis. Six genes (CHMP7, GSDME, GZMB, CASP9, IL6, and NLRP1) were obtained by Lasso Cox regression analysis to construct a prognostic model. The high-risk group had a poor prognosis with areas under the ROC curve at 1-, 3-, and 5-years of 0.619, 0.692, and 0.656, respectively. Univariate and multivariate Cox analyses showed that the risk score was an independent prognostic factor. Enrichment analysis of GO and KEGG pathways revealed that differentially expressed genes may be related to infection, T cell differentiation, immunity, and inflammation. It was further found that the low survival rate of the high-risk group may be related to the significant reduction of immune cell infiltration and immune function. With the bioinformatic method, six genes related to pyroptosis affecting LC prognosis were screened and a prognostic risk model was constructed, which laid a foundation for pyroptosis study in LC.

Keywords: Pyroptosis, laryngeal carcinoma, prognosis, Lasso Cox regression, gene expression

Introduction

Laryngeal carcinoma (LC) has remained one of the most common malignant tumors of the respiratory tract in the last 40 years, with the five-year survival rate dropping from 66% to 63% [1], although the incidence of LC has been declining slowly [2]. Since the symptoms of early stage LC are similar to those of chronic laryngitis, such as chronic pain in the throat, hoarseness, sore tongue, and non-healing ulcers [3], most patients are diagnosed in the middle and advanced stages, resulting in limited treatment options. A plausible effective avenue to decrease the incidence of LC seems to be early diagnosis and prompt treatment. Although many approaches, including fiberoptic endoscopy, computed tomography (CT), magnetic resonance imaging (MRI), positron emission tomography (PET) scan, p16 immunohistochemistry (IHC), and tumor programmed death-ligand 1 (PD-L1), have been extensively applied in the diagnosis [1, 3], their clinical benefits are still limited by the high cost of the tests and uncertainty with indicators for the early stage of LC. Currently, radical resection, radiotherapy, and chemotherapy are the mainstay curative treatments for LC. Although there is a certain probability of cure, such multi-mode treatment often leads to further deterioration of swallowing, breathing, and voice function, which seriously reduces the quality of life. Therefore, seeking accurate and reliable diagnosis and treatment strategies for patients with LC is a major challenge.

Cell death is a protective mechanism that helps the body eliminate endogenous and exogenous injury, thus maintaining normal tissue function and morphology. The modalities of cell death

are diverse, including but not limited to apoptosis, necroptosis, pyroptosis and ferroptosis, which play a vital role in tissue regeneration, infection, immunity, and tumorigenesis. As the most classic programmed cell death (PCD) process, apoptosis is an active mechanism in response to stress-inducing or regulatory signals induced by cysteine protease. Similarly, pyroptosis is also a caspase-dependent PCD mode that has been discovered in recent decades and is mainly driven by pore formation proteins of the Gasdermin (GSDM) family [4]. Members of the GSDM family have C-terminal and N-terminal domains, and GSDM can be cleaved to release the GSDM-N domains, resulting in a large number of pores on the cell membrane and osmotic swelling of the cell [5, 6]. In the late stage of pyroptosis, swollen cells eventually disintegrate, release inflammatory contents, rapidly stimulate the inflammatory response of the body, and finally cause cell swelling and death. Since Cookson et al. first named this type of PCD as pyroptosis in 2001 [7], pyroptosis has been considered as an inflammatory cell death mode solely dependent on caspase-1 activity. However, in the past few decades, an increasing number of studies have shown that pyroptosis is closely associated with many diseases, such as myocardial infarction [8], cirrhosis [9], and sepsis [10]. In addition, the research on pyroptosis in tumors is advancing, the expression of pyroptosis-related factor has been proven to be highly correlated with a variety of cancers [11]. Pyroptosis per se and pyroptosis-induced signaling molecules and cytokines inhibit the proliferation and metastasis of tumor cells. Thus, it may be an effective target for tumor therapy and provide some use for clinical treatment. Pyroptosis is also closely related to immune function. GSDME has been reported to inhibit tumor cell growth by enhancing anti-tumor adaptive immunity [12], and by regulating the tumor immune microenvironment [13]. Furthermore, in head and neck squamous cell carcinoma (HNSCC), reduced expression of the calcium regulatory factor CD38 can prevent inflammasome-induced pyroptosis and may play a tumor suppressive role in the progression [14]. Some natural medicines such as triptolide may eliminate HNSCC cells by inducing GSDME-mediated pyroptosis [15]. The emergence of pyroptosis-associated therapy offers the possibility of long-term remission of refractory and/or metastatic carcinoma [16]. However, data on the studies on LC-related pyroptosis are limited. Therefore, there is an urgent need to explore the relationship between pyroptosis and LC, to provide more possibilities for early diagnosis and treatment.

In this study, to assess the prognostic value of pyroptosis in LC, we used gene expression profiling data as well as clinical data from LC and normal tissue samples from the Cancer Genome Atlas (TCGA) and Gene Expression Omnibus (GEO) databases. We determined the association between pyroptosis-related genes and patients' clinicopathologic factors. Furthermore, we constructed and validated a prognostic model of pyroptosis-associated genes and performed tumor immune microenvironment analysis. In summary, our results indicated that pyroptosis might be closely related to LC, and this prognostic model could be used to predict the prognosis of patients with LC.

Materials and methods

Data acquisition

Gene expression data from LC (355 samples of LC and 31 normal samples, type: HTSeq - FPKM) and corresponding clinical information (376 cases) were downloaded from the TCGA database. Accordingly, another set of data (183 samples screened from 270 HNSCCs of the queue. ID: GSE65858) was downloaded from the GEO database.

Identification of differentially expressed pyroptosis-related genes

Referring to the previous review and the GeneCards database [4, 5, 11, 17], 52 genes related to pyroptosis were obtained by virtue of the following inclusion criteria: 1) Genes involved in the molecular mechanism of pyroptosis; 2) Genes associated with pyroptosis act as a pivotal part in tumors; 3) The data recorded in the experimental study are complete; 4) Genes are identified to be associated with pyroptosis in the GeneCards database. Exclusion criteria: 1) Genes not clearly related to pyroptosis; 2) Incomplete or doubtful data. Then, the "limma" package of R software was used to find the expression level of pyroptosis-related genes. The "pheatmap" package was used to draw heatmaps for the visualization of

differentially expressed genes (DEGs). The protein-protein interaction (PPI) network of DEGs was downloaded from STRING online software. We also constructed a co-expression network using the "reshape2" and "igraph" packages of R software.

Consensus clustering

To explore whether pyroptosis-related genes are associated with prognosis, we performed consensus clustering using the "ConsensusClusterPlus" package of R software. To assess the stability of our classification, 1000 repetitions were analyzed according to the methods described previously.

Construction and validation of a DEG prognostic model

To explore whether DEGs were associated with prognosis, we combined the expression levels of DEGs with the survival information of LC samples. After excluding patients without survival, 376 cases of LC were included in Cox regression analysis. The "glmnet" package of R software was utilized to conduct Lasso Cox regression analysis for the screening of candidates. Construction of a DEG prognostic model was done by assessing the prognostic value of differential genes obtained by univariate Cox analysis. The penalty parameter (λ) was determined using the minimum standard and the risk score of the DEG prognostic model was computed by the formula: Risk score = gene expression 1 × Coef1 + gene expression 2 × Coef2 +... + gene expression n× Coefn (Coef: regression coefficient of gene, n: total number of DEGs associated with prognosis). With reference to the guide of polygenic risk score analyses and a similar study [18, 19], risk scores were calculated after centralizing and normalizing the TCGA expression data, and patients with LC were divided into high-and low-risk groups according to the median risk scores. "Survival" package and "survminer" packages of R software were used to draw Kaplan-Meier survival curves. "Rtsne" package and "ggplot2" packages were used for the principal component analysis (PCA) and t-distributed stochastic neighbor embedding (t-SNE) analysis. Time receiver operating curve (ROC) analysis was conducted using "time ROC" package, and the area under curve (AUC) was calculated at 1, 3, and 5 years for the evaluation of the model's ability to predict prognosis. Then, GSE65858 was selected as the external validation set in the GEO database, and the risk score of each sample in the validation set was calculated according to the above risk scoring formula. The Kaplan-Meier survival curve was used to compare the overall survival (OS) of the two groups and to evaluate the prognostic ability of the model, to verify its performance.

Independent prognostic analysis of the prognostic model

We extracted clinical data (including age, gender, grade, and T stage, et al.) of LC patients from the TCGA and GEO databases. Combined with the risk score in the prognostic model, univariate and multivariate Cox regression analyses were used to analyze the risk score of the prognostic model, and forest plots were drawn to explore the predictive ability of prognostic model for clinical features.

Functional enrichment analysis and ssGSEA analysis of the DEGs between the low- and high-risk groups

According to the risk model, the DEGs of patients in the high- and low-risk groups were calculated, and gene ontology (GO) analysis was performed to obtain the enrichment of DEGs related to the biologic processes, molecular functions, and cellular components. Kyoto encyclopedia of genes and genomes (KEGG) analysis was also performed to identify differential gene enrichment signaling pathways. GO and KEGG analyses were implemented through the "clusterProfiler" package of R software. Finally, Single-sample gene set enrichment analysis (ssGSEA) was performed with the "gsva" package to calculate the score of infiltrating immune cells and assess the activity of immune-related pathways.

Statistical analysis

All statistical analyses were accomplished with the R software (version 4.1.0). Kaplan-Meier analysis was used to perform survival analysis and plot the survival curves. Univariate and multivariate Cox regression analyses were used to determine the prognostic factors and establish risk scoring formulas. Lasso Cox regression analysis was used to construct a prognostic risk model. The efficacy of the prognostic model

was evaluated using an ROC curve. The classification variables were evaluated using Pearson correlation analysis.

Mann-Whitney test was applied to compare immune cell infiltration and immune pathway activation

Results

Identification of DEGs between LC and normal tissues

After we extracted the expression levels of pyroptosis-related genes, 37 DEGs were identified. Among them, 31 genes (NLRP6, NLRC4, CASP5, CHMP4A, NOD1, NLRP7, SCAF11, GSDMB, TNF, CASP8, CHMP7, NLRP1, CASP6, IRF2, CASP3, PLCG1, CASP1, GSDME, HMGB1, IRF1, GZMB, GZMA, GSDMD, IL1B, AIM2, BAX, PYCARD, BAK1, CHMP4B, IL1A, TP63) were upregulated in the tissue samples, and 6 genes (IL6, IL18, CHMP2B, CHMP6, ELANE, CASP9) were downregulated, as shown in **Figure 1A**. In addition, PPI analysis was conducted using the online STRING website. As shown in **Figure 1B**, CASP1, 1L1B, PYCARD, CASP8, NLRC4, and AIM2 are the core genes in the network, which are all DEGs in tumor and normal samples. In addition, the correlation network analysis containing all DEGs was also conducted, and obvious positive or negative correlation between two of any DEGs was identified in the network (**Figure 1C**).

Consensus clustering based on DEGs

We conducted a consensus clustering analysis on 355 LC patients in the TCGA cohort. When K = 2, the intra-group correlation was the highest, and the clustering result was the best. It was suggested that 355 patients with LC could be divided into two groups based on 37 DEGs (**Figure 2A**). The gene expression profile and clinical findings, such as the phase of tumor metastasis (N0-N1, M0-M1, T1-T4), clinical stage (stage I-stage IV), the degree of tumor differentiation (G1-G4), gender (female or male) and age (≤65 or >65 years) were presented in a heatmap in terms of the clustering of LC patients. To examine the clinical significance in the clustering of LC subtypes, these clinical findings were compared between two clusters using Pearson correlation analysis. A significant difference was found in the phase of tumor metastasis including T stage ($P < 0.05$) and grade ($P < 0.001$), and most of the DEGs were up-regulated in cluster2, as shown in **Figure 2B**. Finally, a significant difference was observed with the manifestation of the superiority of survival status of cluster2 over that of cluster1 ($P = 0.006$. **Figure 2C**), suggesting that pyroptosis-related genes had significant prognostic value.

Construction of the pyroptosis-related genes prognostic model

Through univariate Cox regression analysis, 8 genes were extracted from the 37 DEGs (**Figure 3A**). Lasso Cox regression analysis was performed on the above 8 genes with significant differences, and cross-validation was used to establish the model, to avoid over-fitting of pyroptosis-related genes. The results showed that the model had the smallest deviation when the number of variables was 6 (**Figure 3B**, **3C**). Then, the risk score prognostic model was successfully constructed, which consisted of the expression levels and coefficients of the above 6 genes. The risk scoring formula was as follows: risk score = (CHMP7 expression level * -0.1703) + (GSDME expression level * 0.1658) + (GZMB expression level * -0.1247) + (CASP9 expression level * -0.0193) + (IL6 expression level * 0.0689) + (NLRP1 expression level * -0.2006). The survival status and corresponding gene expression levels of 353 LC patients were obtained by collating clinical sample data downloaded from the TCGA database. After calculating the risk score according to the formula of risk score, patients were divided into high- and low-risk groups according to the median value (-0.625), including 176 patients in the high-risk group and 177 patients in the low-risk group (**Figure 3D**). Survival curve in Kaplan-Meier analysis evidenced a significant difference of OS time between the two groups, confirming higher survival probability in the low-risk group than that of the high-risk group ($P < 0.001$. **Figure 3F**). With an increase in the risk score, the mortality rate of patients with LC gradually increased (**Figure 3E**). ROC curve analysis showed that the model had a good effect in predicting the prognosis and survival of patients with LC, and the AUCs at 1, 3, and 5 years were 0.619, 0.692, and 0.656, respectively (**Figure 3G**). PCA and t-SNE analyses also fully confirmed the classification ability of the

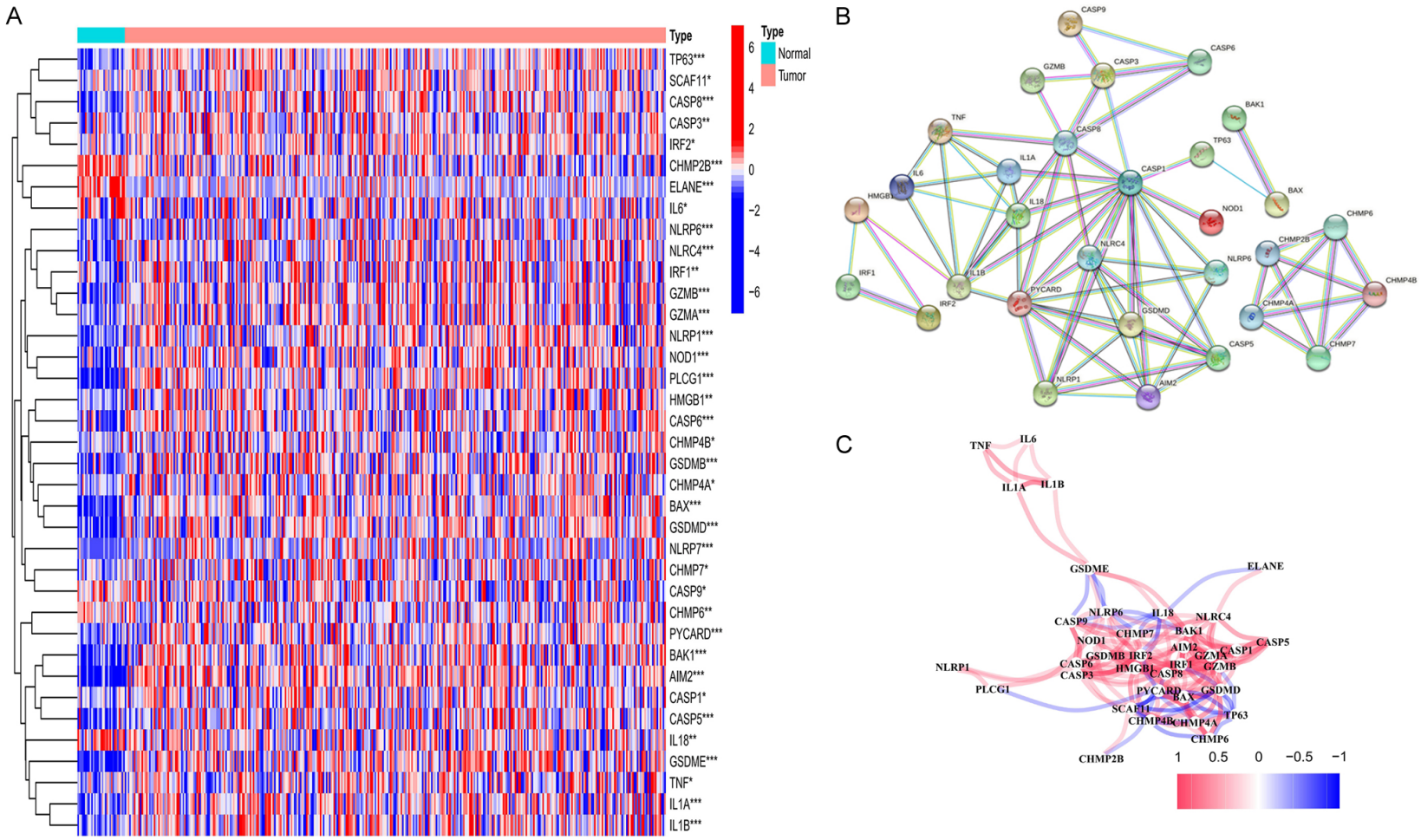

Figure 1. Expressions of the 37 pyroptosis-related genes and the interactions among them. A. A heatmap was used to show the expression levels of DEGs between normal and tumor tissues (blue: low expression. red: high expression. *P* values are marked as: *P < 0.01; **P < 0.01; ***P < 0.001). B. PPI network of the relationship between pyroptosis-related genes (interaction score = 0.9). C. Interrelationships among pyroptosis-related genes (red line: positive correlation; blue line: negative correlation).

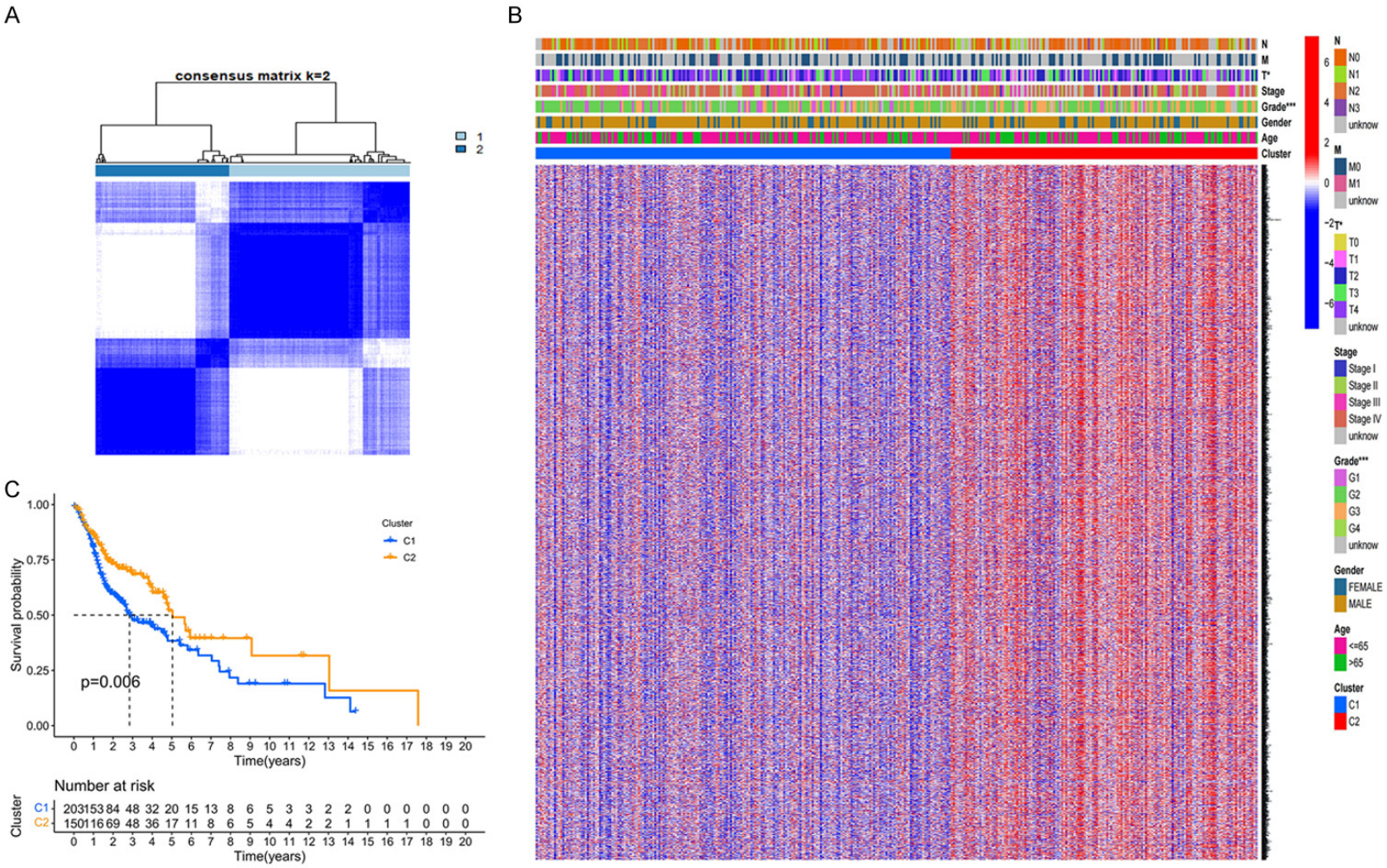

Figure 2. Consensus clustering based on DEGs. A. According to the consistent clustering matrix (k = 2), 355 patients with LC could be well divided into two clusters. B. Heatmap of the gene expression signatures and clinicopathological features for the two clusters. C. Kaplan-Meier survival curves for the two clusters.

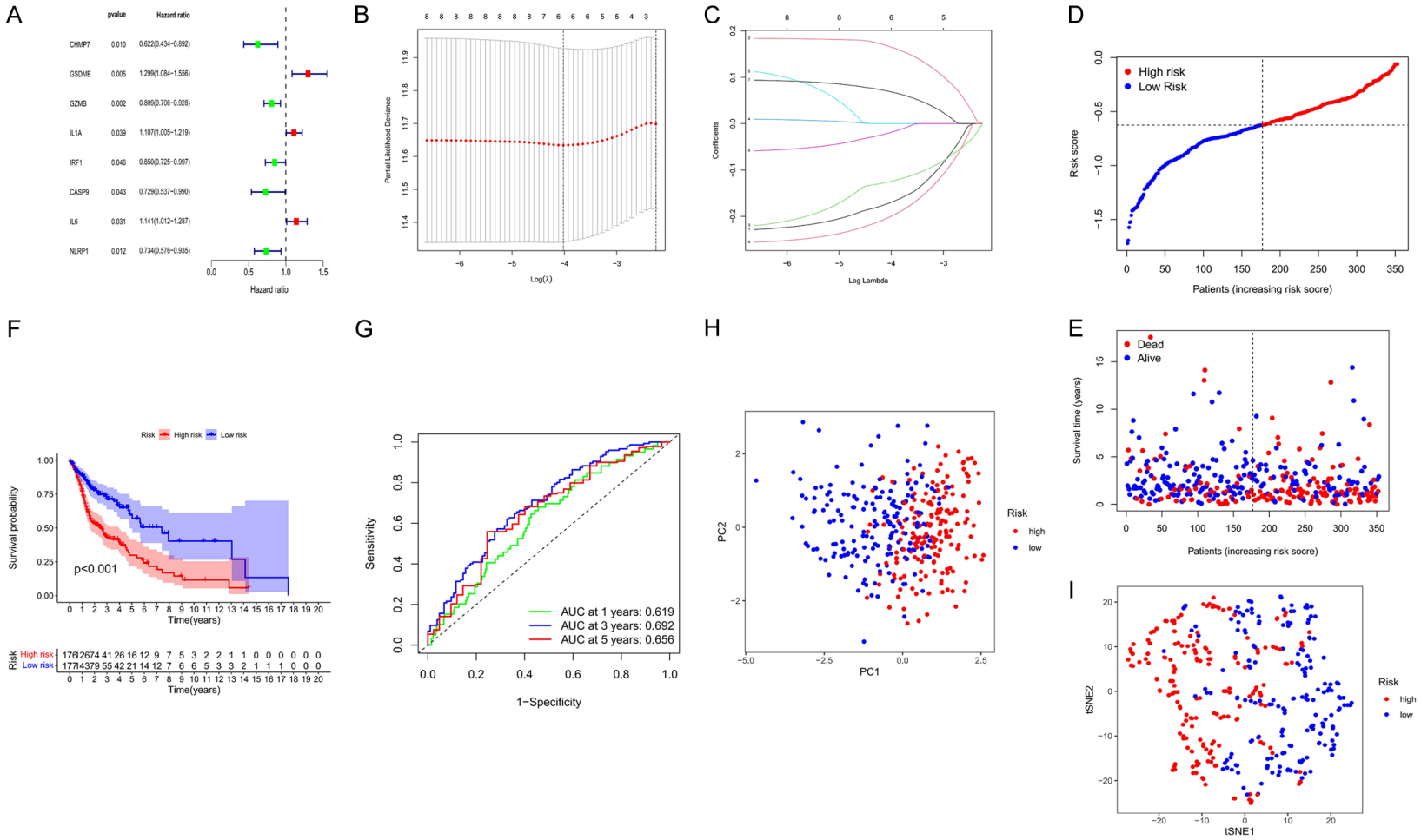

Figure 3. Construction of the pyroptosis-related gene prognostic model. A. Univariate Cox regression analysis was used to assess DEGs of LC samples from the TCGA cohort, and 8 genes were screened out based on P < 0.05. B. Cross validation of the 8 genes for tuning the parameter selection in the Lasso regression. C. Lasso coefficients of the 8 genes in LASSO Cox regression for the construction of risk scoring formula. D. Distribution of patients based on the risk score. E. Survival status of patients in the high (on the right side of the dotted line) and low (on the left side of the dotted line) risk groups. F. Kaplan-Meier survival curves. G. ROC curve analysis. H. PCA plot based on the risk score. I. t-SNE plot based on the risk score.

model for high and low risk groups (**Figure 3H**, **3I**).

External validation of the prognostic model

We next selected the cohort of 183 LC patients from the GEO database (ID: GSE65858) to verify the model. The calculation method of the prognostic risk score and the grouping method of patients with high and low risk remained unchanged. These patients were clustered into two groups, with 176 in the low-risk group and 7 in the high-risk group (**Figure 4A**). The Kaplan-Meier survival curve showed that the OS of patients in the high-risk group was significantly shortened (P = 0.047. **Figure 4B**), suggesting that the model had the same prognostic risk assessment ability for patients with LC in an external independent cohort. The analysis by ROC curve showed an AUC of 0.638 for 1 year, 0.600 for 3 years, and 0.566 for 5 years respectively (**Figure 4C**). As the risk score increased, the survival time gradually decreased (**Figure 4D**), and PCA and T-SNE analyses also showed the same trend with the TCGA cohort (**Figure 4E**, **4F**).

Independent prognostic value of the prognostic model

We next investigated whether risk score originating from the DEG prognostic model could act as an independent predictive factor for survival status of LC patients. Univariate Cox regression analysis showed that the risk score could be an independent prognostic factor in both groups (TCGA cohort: P < 0.001, HR = 3.742, 95% CI = 1.921-7.289, **Figure 5A**. GEO cohort: P = 0.007, HR = 3.543, 95% CI = 1.422-8.827, **Figure 5C**). Multivariate Cox regression analysis showed that the risk score was still an independent prognostic factor (TCGA cohort: P < 0.001, HR = 3.540, 95% CI = 1.789-7.003, **Figure 5B**. GEO cohort: P = 0.010, HR = 3.449, 95% CI = 1.347-8.827, **Figure 5D**). Besides, combined with univariate and multivariate Cox regression analyses, it was observed that age and N stage were also significantly associated with the prognosis of patients with LC in the TCGA cohort (P < 0.01, **Figure 5A**, **5B**). In the GEO cohort, T stage was significantly correlated with prognosis of patients (P < 0.05, **Figure 5C**, **5D**). In addition, the heatmap that integrated the DEG signature and clinical findings of LC patients in the TCGA cohort revealed a significant difference of clinical grade of tumor differentiation and T stage between the low- and high-risk groups (P < 0. 05. **Figure 5E**).

Functional analyses based on the prognostic model

According to the risk score of the prognostic model, we selected 47 DEGs according to FDR < 0.05, and |log2FC| ≥1 in the TCGA cohort. GO and KEGG analyses were performed based on these DEGs. GO enrichment analysis showed that the DEGs were highly enriched in cell differentiation, T cell activation, and MHC protein complexes (**Figure 6A**). KEGG enrichment analysis showed that these DEGs were correlated with infection, T cell differentiation, immunity, and inflammation (**Figure 6B**).

Comparison of the immune activity between high and low risk groups

To compare immune cell infiltration and activation of immunity-related functions, ssGSEA analysis was performed on the high- and low-risk groups in the TCGA and GEO cohorts. The results showed that the high-risk group generally had a low level of immune cell infiltration in the TCGA cohort. It was mainly manifested in the antibody drug conjugates (aDCs), B cells, $CD8^+$ T cells, mast cells, natural killer (NK) cells, plasmacytoid dendritic cells (pDCs), T helper cells (Tfh, Th1 cells, Th2 cells), and regulatory T(Treg) cells (**Figure 7A**). In all 12 immune pathways except the major histocompatibility complex (MHC) class1, the high-risk group had significantly lower levels than the low-risk group (**Figure 7B**). In the GEO cohort, $CD8^+$ T cells, mast cells, NK cells, and pDCs were lower in the high-risk group than in the low-risk group (**Figure 7C**). Cytolytic activity, inflammation promotion, MHC class1, anaphase promoting complex (APC) co-inhibition, checkpoint, and T cell co-inhibition were lower in the high-risk group than in the low-risk group (**Figure 7D**). This indicated that the prognostic model effectively disclosed the status of the immune microenvironment.

Discussion

Laryngeal carcinoma (LC) is a malignant tumor that reduces the quality of life. Despite great advances in diagnosis and treatment in recent years, the survival rates remain poor. Since the

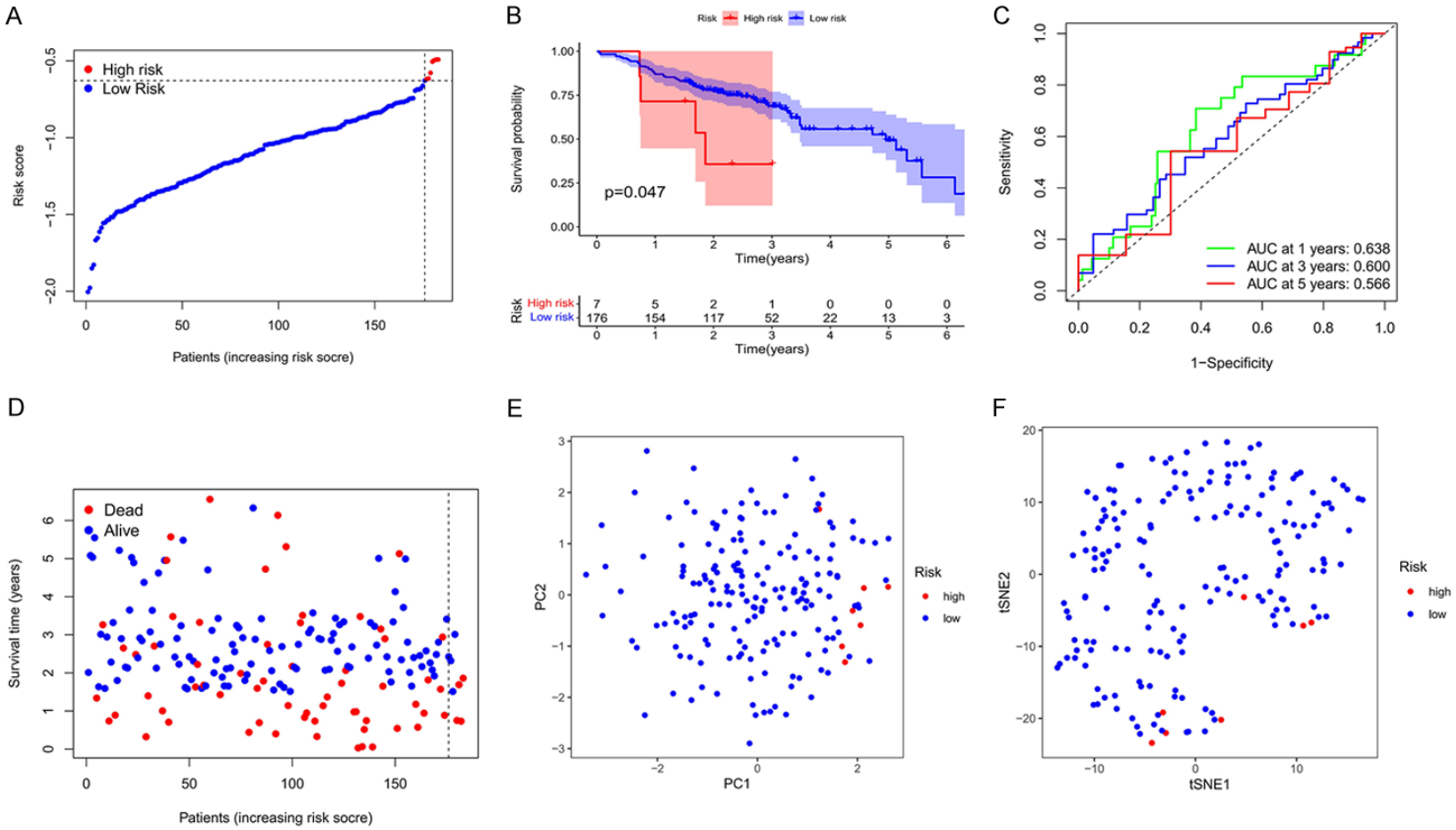

Figure 4. Validation of the prognostic model in the GEO cohort. A. Distribution of patients in the GEO cohort based on the median risk score in the TCGA cohort. B. Kaplan-Meier curves between low- and high-risk groups. C. ROC curves of the risk score in the GEO cohort. D. The survival status for each patient in the high- and low-risk groups. E. PCA plot. F. t-SNE analysis.

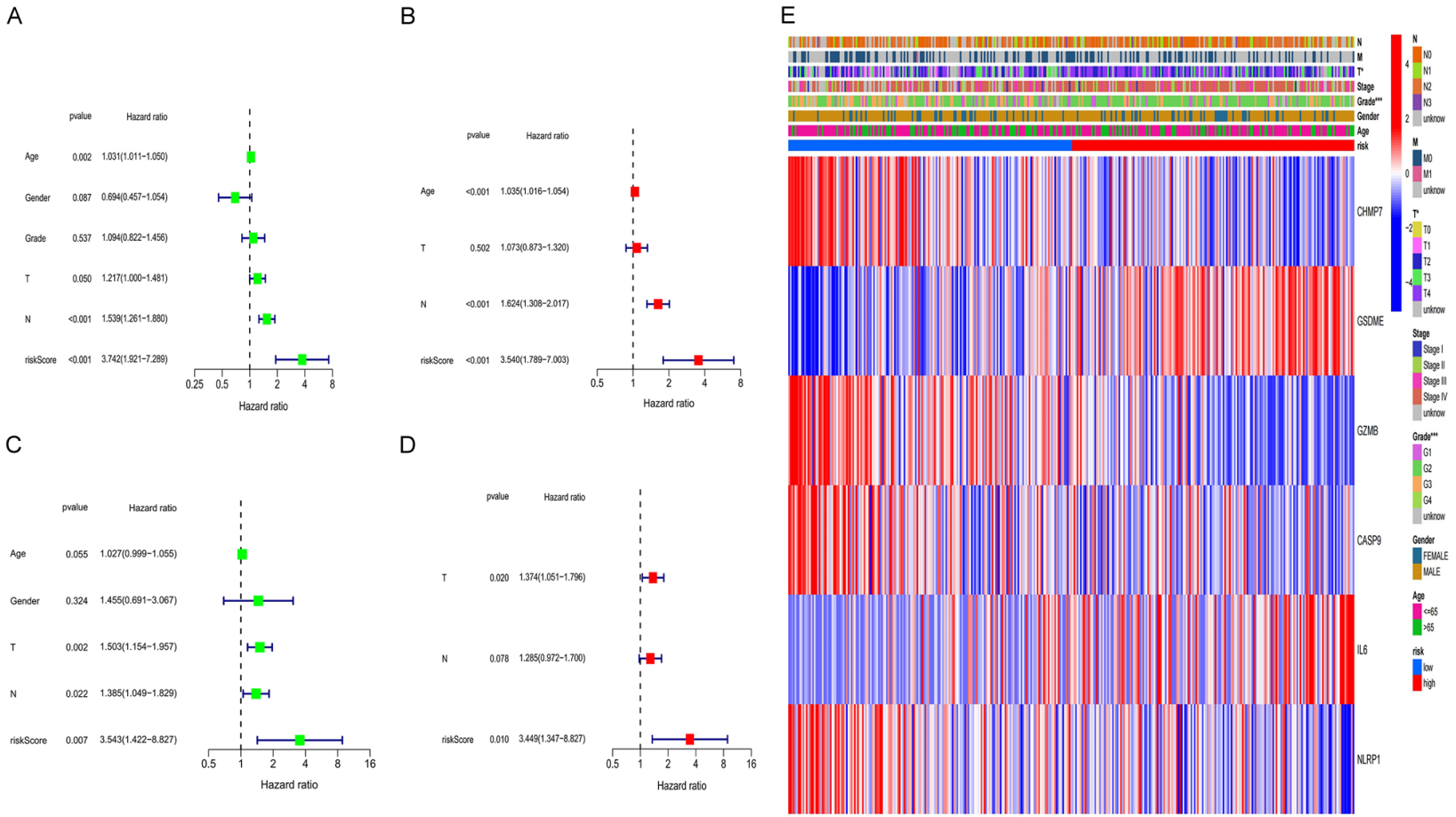

Figure 5. Univariate and multivariate Cox regression analyses for the risk score. (A) Univariate and (B) Multivariate analysis, respectively, for the TCGA cohort. (C) Univariate and (D) Multivariate analysis, respectively, for the GEO cohort. (E) Heatmap of the gene expression signatures and clinicopathological characteristics for high and low risk groups (blue: low expression; red: high expression).

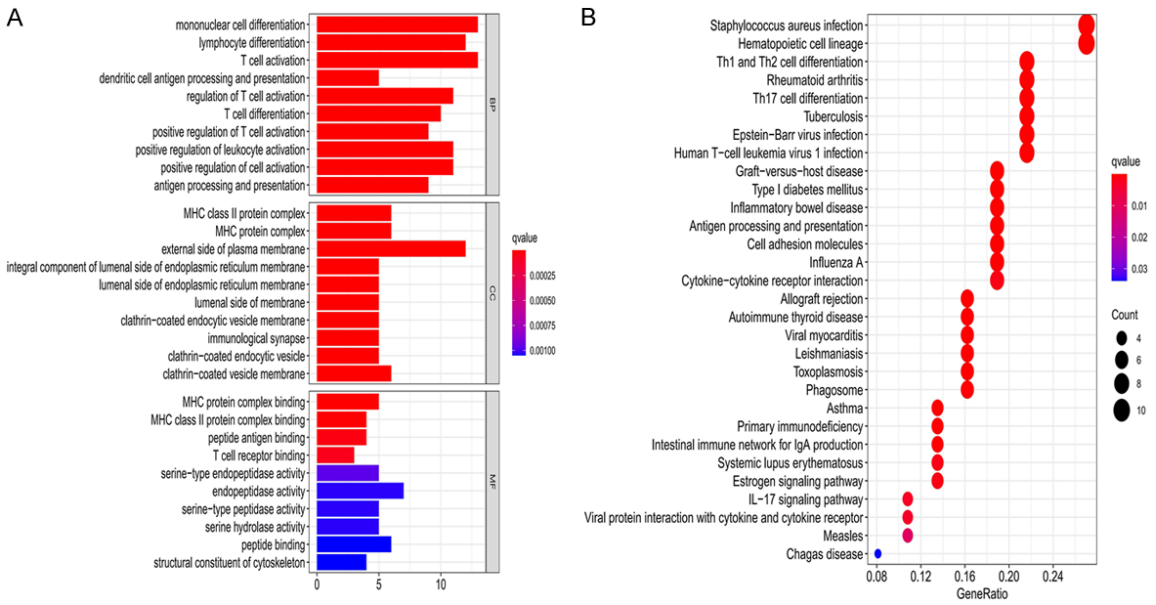

Figure 6. Functional analyses based on the prognostic model in the TCGA cohort. A. GO enrichment analysis barplot graph of DEGs (color represents q value, the daker the color, the more significant the difference; The length of the bar represents the degree of enrichment; q value: the adjusted *p* value). B. GO enrichment bubble graph of the DEGs (The bubble size of the bubble graph represents the degree of enrichment).

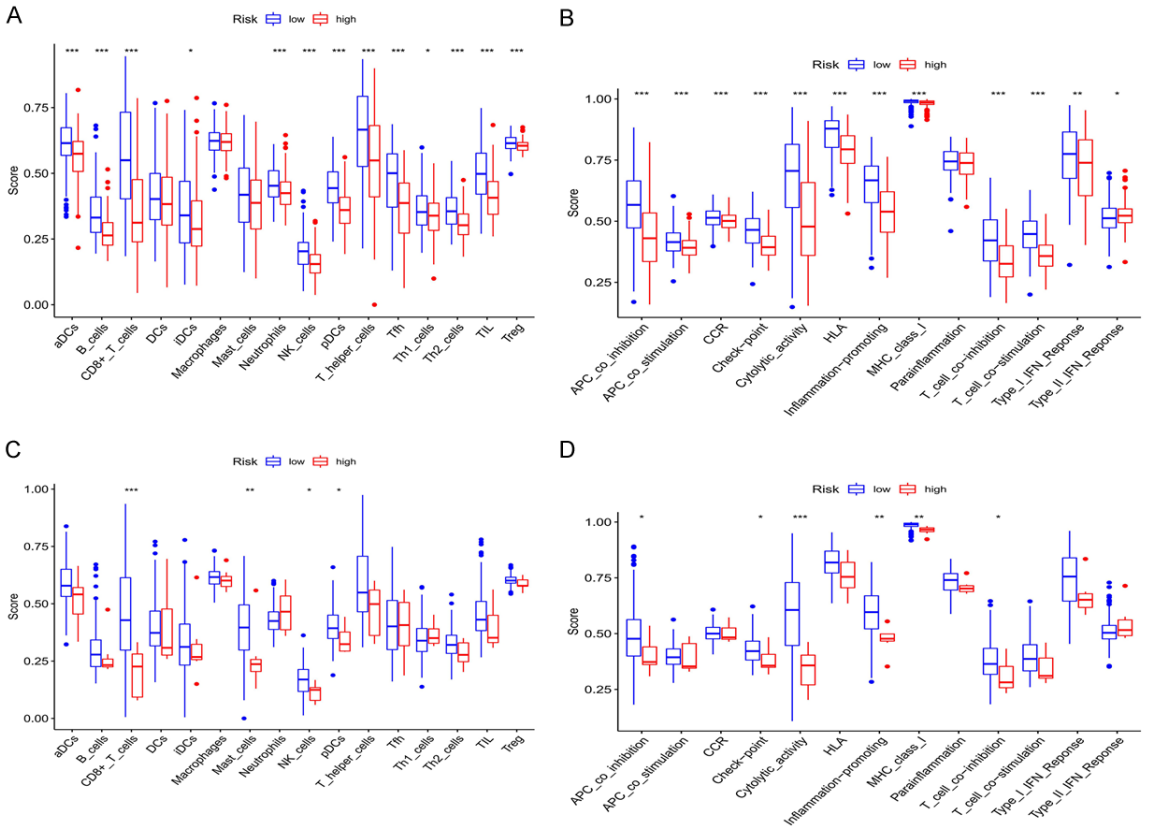

Figure 7. Comparison of the ssGSEA scores for immune cells and immune pathways. A, B. Differences in the enrichment scores of immune cells and immune-related pathways between the high and low risk groups in the TCGA cohort. C, D. Differences in the enrichment scores of immune activity between the high and low risk groups in the GEO cohort. *P* values are marked as: *P < 0.05; **P < 0.01; ***P < 0.001.

main purpose of cancer treatment is to trigger the death of cancer cells, the anti-apoptotic properties of tumor cells often lead to treatment failure. Thus, it is important to explore the mechanism of non-apoptotic programmed cell death in tumor therapy, and pyroptosis is a new discovery. Although the tumor-promoting role of pyroptosis in cancer has been demonstrated in many studies, such as in colorectal cancer, recent studies have shown that inducing pyroptosis may trigger a powerful anti-tumor effect, such as in hepatocellular carcinoma [4]. Since tumor cells have an innate anti-apoptotic ability, inducing pyroptosis may be of great value for the treatment of tumors [20]. Therefore, it is of great value to explore the relationship between LC and pyroptosis. In this study, 6 key DEGs that were significantly associated with LC were screened based on pyroptosis-related genes, and a predictive model of LC prognosis was constructed based on the DEGs. The validation showed that the model had a good predictive efficiency.

In addition, we performed both a retrospective study of patients with LC and a comprehensive and detailed assessment of pyroptosis-related genes to explore their association with survival and clinicopathological characteristics. First, we found that 37 pyroptosis-related genes were differentially expressed in tumor and normal tissues. Consistent clustering and survival analysis showed that DEGs could be used to predict the prognosis of patients with LC. The 6 genes (CHMP7, GSDME, GZMB, CASP9, IL6, and NLRP1) were further screened to construct a prognostic model using Cox regression and Lasso Cox regression analyses. CHMP7 (charged multivesicular body protein 7) is a protein-coding gene related to cellular senescence. During cell division, the macromolecular O-ring formed by the co-assembly of CHMP7 and LEM2 is associated with the nuclear envelope reformation [21]. Excessive activation of CHMP7 reduces translation efficiency [22] and may lead to severe membrane deformation, and further affects cell growth, metabolism, division, and internal environment stability [23]. In recent years, although a genetic association study has shown that CHMP7 is associated with gastric cancer [24], the role of CHMP7 in tumors remains unclear. However, the activation of the ESCRT-III mechanism involved in CHMP7 is associated with cancer cell death resistance, especially with the use of anticancer drugs [25], which may have potential for cancer treatment. GSDME is an important member of the GSDM family. As a key substrate for regulating pyroptosis, the GSMD family plays a key role in both classical and non-classical pathways of pyroptosis, among which GSDME and GSMDB are the two most widely expressed and studied [26]. In short, GSDME transforms caspase-3-mediated apoptosis into pyroptosis or causes cells to go directly to pyroptosis [27]. On the one hand, GSDME activates antitumor immunity to suppress tumor growth by increasing the number of cytotoxic lymphocytes [28]. On the other hand, GSDME has also been found to be related to the immune escape of tumor cells. Abnormal methylation of DNA in the GSDME promoter region in most tumor cells leads to low expression or silencing of GSDME. In these cells, caspase-3 activated by anti-tumor drugs cleaves the downstream apoptotic protein PARP instead of GSDME to initiate apoptosis. Accordingly, methylation inhibitors restart the GSDME's pyroptosis process to achieve the goal of cancer treatment [26, 28]. Surprisingly, we found that GSDME was highly expressed in LC tissues. We further hypothesized that abundant inflammatory factors released by GSDME-induced pyroptosis may promote the occurrence of LC and lead to poor prognosis. This seems to be contrary to the GSDME-inhibitory or silencing properties of most tumors. Therefore, the significance of GSDME in the development and treatment of LC needs to be further explored. Granzyme B (GZMB), a unique immune defense effector protease is stored in the secretory vesicles of killer cells. After secreting cytosolic granules during killer cell attack, GZMB is transported to the cytoplasm of target cells with the help of the pore-forming protein perforin, activating the primary executor apoptosis pathway [29]. As an important effector molecule of natural killer cells, GZMB enhances the cytotoxic activity of $CD4^+$ T cells against tumors [30]. Tumor cells have a self-protection mechanism by blocking the mitochondrial death pathway activated by GZMB. Thus, activating GZMB expression and modulating immunity may be an important direction in tumor therapy [31]. In addition, GZMB induces GSDME-dependent pyroptosis in tumor targets by directly cleaving GSDME and indirectly by activating caspase-3 [28], which is consistent with the results of our

co-expression network. Interestingly, our results suggested that GZMB was highly expressed in LC tissues and may be an oncogenic gene, but it was enriched in the low-risk group and could prolong the survival of patients. This is worthy of further study. Caspase 9 (CASP9) is a key promoter of apoptosis and has been proven to be associated with HNSCC [32]. Recent studies have shown that upregulation of CASP9 contributes to TNFα promoting apoptosis of cancer cells [33]. Targeting CASP9 signaling in combination with radiotherapy and immune checkpoint blocking can effectively control tumors by sequentially blocking endogenous and exogenous inhibitory signals [34]. This could lead to new strategies for cancer treatment. Interleukin-6 (IL6) is an inflammatory cytokine involved in a variety of biologic processes, including immune disorders and cancer. Anti-IL6 therapy has been used in the treatment of multiple myeloma, prostate cancer, hematologic tumors, and renal cell carcinoma [35]. NLRP1 is the first protein identified to be assembled into an inflammatory complex and is primarily involved in autoimmunity, autoinflammation, and other diseases. Recent studies have found that NLRP1 activation leads to downstream chemokine production and induces pyroptosis, which appears to be a protective mechanism, such as the improved resistance to Bacillus anthracis [36, 37]. In our study, we found that NLRP1 was highly expressed in the low-risk group, which was consistent with a protective mechanism of NLRP1-induced pyroptosis. However, NLRP1 was highly expressed in tumor tissues, whether it is an oncogene is uncertain.

In summary, the 6 genes associated with the prognostic model (CHMP7, GSDME, GZMB, CASP9, IL6, and NLRP1) are promoters of pyroptosis, control genes of apoptosis, or key factors in the inflammatory response. It is generally believed that blocked apoptosis leads to excessive proliferation of tumor cells during tumorigenesis. Initiating pyroptosis may be an effective means of treating cancers. Nonetheless, pyroptosis caused by inflammation may promote the development of tumor. Therefore, further studies on pyroptosis are needed to better understand the occurrence, development, and treatment of tumors.

Validation of the prognostic model using the GEO database demonstrated that the model could effectively predict the prognosis of patients with LC. Independent prognostic analysis also demonstrated that the risk score could be used as an independent prognostic factor. To evaluate the expression of differential genes in the high- and low-risk groups, we performed GO and KEGG analyses, and the results showed that the differentially expressed genes were highly enriched in cell differentiation, T cell activation and differentiation, MHC protein complex, infection, immunity, and inflammation. Therefore, we believe that inflammation and immune cell infiltration are key factors in different risk groups, and that changes in the tumor microenvironment associated with pyroptosis may be key factors influencing prognosis. Therefore, we performed immune cell infiltration and immune function analysis.

The rapid proliferation of tumor cells is due to their ability to modulate the surrounding environment to favor their own proliferation. The internal environment that favors their biological behavior is called the tumor microenvironment. We found that the high-risk group had a lower level of immune cell infiltration and immune functions than the low-risk group, and the samples from the GEO database also reached a consistent conclusion, suggesting that the poor prognosis of patients in the high-risk group may be caused by the overall reduction in immune levels. Recent research also proved that immunosuppression and immune escape play a vital role in tumorigenesis, in which tumor cells can express immune-inhibitory molecules to evade immune attacks from the host [38]. Our study confirmed this conclusion, and also identified new immune targets associated with the prognosis of LC, which are expected to provide a basis for future clinical trials and individualized treatment.

Pyroptosis may be a double-edged sword for cancer patients. In order to explore the role of pyroptosis in various cancers, the most direct and specific method is to develop prognostic and diagnostic models related to pyroptosis. Currently, the role of pyroptosis in LC remains unknown, and our findings contribute to the development of accurate and sensitive diagnostic and prognostic biomarkers for LC. Although we have conducted multi-angle and multi-database validation, there are still limitations to this study that need to be considered. Our prognostic model needs to be validated

with reliability and accuracy in more external data sets and large clinical cohorts. Second, the mechanism of the precise process of pyroptosis regulation of LC remains unclear. In addition, the mechanism of the prognostic model on LC immunotherapy is also unknown, which needs to be clarified in further research. The recent development of various pyroptosis-inducing cancer drugs points the way forward for cancer therapy [39]. In the future, we will build upon previous progress to further explore the mechanism of pyroptosis-related genes and prognostic models in LC.

Conclusion

Through the joint analysis of data from the TCGA and GEO databases, this study successfully constructed a prognostic risk assessment model for LC mediated by 6 pyroptosis-related genes, which may well predict the prognosis of patients with LC. The screened genes might be new targets for LC diagnosis and treatment, and are expected to provide theoretical support for the study of pyroptosis-related molecular mechanisms and prognosis of LC.

Acknowledgements

This work was supported by the National Natural Science Foundation of China (No. 82074581).

Disclosure of conflict of interest

None.

Address correspondence to: Yu Guo, Department of Otolaryngology, Shanghai Municipal Hospital of Traditional Chinese Medicine, Shanghai University of Traditional Chinese Medicine. No. 274, Zhijiang Middle Road, Jing'an District, Shanghai, China. Tel: +86-18116013560; E-mail: gyszyent@163.com

References

[1] Steuer CE, El-Deiry M, Parks JR, Higgins KA and Saba NF. An update on larynx cancer. CA Cancer J Clin 2017; 67: 31-50.

[2] Baird BJ, Sung CK, Beadle BM and Divi V. Treatment of early-stage laryngeal cancer: a comparison of treatment options. Oral Oncol 2018; 87: 8-16.

[3] Machiels JP, Rene Leemans C, Golusinski W, Grau C, Licitra L and Gregoire V, EHNS Executive Board. Electronic address: secretariat@ehns.org EEBEa, clinicalguidelines@esmo.org EGCEa and info@estro.org EEBEa. Squamous cell carcinoma of the oral cavity, larynx, oropharynx and hypopharynx: EHNS-ESMO-ESTRO Clinical Practice Guidelines for diagnosis, treatment and follow-up. Ann Oncol 2020; 31: 1462-1475.

[4] Loveless R, Bloomquist R and Teng Y. Pyroptosis at the forefront of anticancer immunity. J Exp Clin Cancer Res 2021; 40: 264.

[5] Li L, Jiang M, Qi L, Wu Y, Song D, Gan J, Li Y and Bai Y. Pyroptosis, a new bridge to tumor immunity. Cancer Sci 2021; 112: 3979-3994.

[6] Wu D, Wei C, Li Y, Yang X and Zhou S. Pyroptosis, a new breakthrough in cancer treatment. Front Oncol 2021; 11: 698811.

[7] Cookson BT and Brennan MA. Pro-inflammatory programmed cell death. Trends Microbiol 2001; 9: 113-114.

[8] Jia XF, Liang FG and Kitsis RN. Multiple cell death programs contribute to myocardial infarction. Circ Res 2021; 129: 397-399.

[9] Soffientini U, Beaton N, Baweja S, Weiss E, Bihari C, Habtesion A, Patel V, Paradis V, Sharma A, Luong TV, Hall A, Nadar A, Sarin S, Chokshi S, Williams R, Py B, Moreau R, Jalan R and Mehta G. The Lipopolysaccharide-Sensing Caspase(s)-4/11 are activated in cirrhosis and are causally associated with progression to multi-organ injury. Front Cell Dev Biol 2021; 9: 668459.

[10] Zheng X, Chen W, Gong F, Chen Y and Chen E. The role and mechanism of pyroptosis and potential therapeutic targets in sepsis: a review. Front Immunol 2021; 12: 711939.

[11] Yu P, Zhang X, Liu N, Tang L, Peng C and Chen X. Pyroptosis: mechanisms and diseases. Signal Transduct Target Ther 2021; 6: 128.

[12] Zhivaki D and Kagan JC. NLRP3 inflammasomes that induce antitumor immunity. Trends Immunol 2021; 42: 575-589.

[13] Erkes DA, Cai W, Sanchez IM, Purwin TJ, Rogers C, Field CO, Berger AC, Hartsough EJ, Rodeck U, Alnemri ES and Aplin AE. Mutant BRAF and MEK Inhibitors regulate the tumor immune microenvironment via pyroptosis. Cancer Discov 2020; 10: 254-269.

[14] Zhang MJ, Gao W, Liu S, Siu SP, Yin M, Ng JC, Chow VL, Chan JY and Wong TS. CD38 triggers inflammasome-mediated pyroptotic cell death in head and neck squamous cell carcinoma. Am J Cancer Res 2020; 10: 2895-2908.

[15] Cai J, Yi M, Tan Y, Li X, Li G, Zeng Z, Xiong W and Xiang B. Natural product triptolide induces GSDME-mediated pyroptosis in head and neck cancer through suppressing mitochondrial hexokinase-Iotalota. J Exp Clin Cancer Res 2021; 40: 190.

[16] Cramer JD, Burtness B, Le QT and Ferris RL. The changing therapeutic landscape of head

and neck cancer. Nat Rev Clin Oncol 2019; 16: 669-683.
[17] Fang Y, Tian S, Pan Y, Li W, Wang Q, Tang Y, Yu T, Wu X, Shi Y, Ma P and Shu Y. Pyroptosis: a new frontier in cancer. Biomed Pharmacother 2020; 121: 109595.
[18] Choi SW, Mak TS and O'Reilly PF. Tutorial: a guide to performing polygenic risk score analyses. Nat Protoc 2020; 15: 2759-2772.
[19] Plath M, Gass J, Hlevnjak M, Li Q, Feng B, Hostench XP, Bieg M, Schroeder L, Holzinger D, Zapatka M, Freier K, Weichert W, Hess J and Zaoui K. Unraveling most abundant mutational signatures in head and neck cancer. Int J Cancer 2021; 148: 115-127.
[20] Raudenska M, Balvan J and Masarik M. Cell death in head and neck cancer pathogenesis and treatment. Cell Death Dis 2021; 12: 192.
[21] von Appen A, LaJoie D, Johnson IE, Trnka MJ, Pick SM, Burlingame AL, Ullman KS and Frost A. LEM2 phase separation promotes ESCRT-mediated nuclear envelope reformation. Nature 2020; 582: 115-118.
[22] Horii M, Shibata H, Kobayashi R, Katoh K, Yorikawa C, Yasuda J and Maki M. CHMP7, a novel ESCRT-III-related protein, associates with CHMP4b and functions in the endosomal sorting pathway. Biochem J 2006; 400: 23-32.
[23] Lusk CP and Ader NR. CHMPions of repair: Emerging perspectives on sensing and repairing the nuclear envelope barrier. Curr Opin Cell Biol 2020; 64: 25-33.
[24] Park SK, Yang JJ, Oh S, Cho LY, Ma SH, Shin A, Ko KP, Park T, Yoo KY and Kang D. Innate immunity and non-Hodgkin's lymphoma (NHL) related genes in a nested case-control study for gastric cancer risk. PLoS One 2012; 7: e45274.
[25] Shahrisa A, Tahmasebi-Birgani M, Ansari H, Mohammadi Z, Carloni V and Mohammadi Asl J. The pattern of gene copy number alteration (CNAs) in hepatocellular carcinoma: an in silico analysis. Mol Cytogenet 2021; 14: 33.
[26] De Schutter E, Roelandt R, Riquet FB, Van Camp G, Wullaert A and Vandenabeele P. Punching holes in cellular membranes: biology and evolution of gasdermins. Trends Cell Biol 2021; 31: 500-513.
[27] Xu W, Che Y, Zhang Q, Huang H, Ding C, Wang Y, Wang G, Cao L and Hao H. Apaf-1 pyroptosome senses mitochondrial permeability transition. Cell Metab 2021; 33: 424-436, e410.
[28] Zhang Z, Zhang Y, Xia S, Kong Q, Li S, Liu X, Junqueira C, Meza-Sosa KF, Mok TMY, Ansara J, Sengupta S, Yao Y, Wu H and Lieberman J. Gasdermin E suppresses tumour growth by activating anti-tumour immunity. Nature 2020; 579: 415-420.
[29] Kurschus FC and Jenne DE. Delivery and therapeutic potential of human granzyme B. Immunol Rev 2010; 235: 159-171.
[30] Sledzinska A, Vila de Mucha M, Bergerhoff K, Hotblack A, Demane DF, Ghorani E, Akarca AU, Marzolini MAV, Solomon I, Vargas FA, Pule M, Ono M, Seddon B, Kassiotis G, Ariyan CE, Korn T, Marafioti T, Lord GM, Stauss H, Jenner RG, Peggs KS and Quezada SA. Regulatory T cells restrain interleukin-2- and blimp-1-dependent acquisition of cytotoxic function by CD4(+) T cells. Immunity 2020; 52: 151-166, e156.
[31] Voskoboinik I, Whisstock JC and Trapani JA. Perforin and granzymes: function, dysfunction and human pathology. Nat Rev Immunol 2015; 15: 388-400.
[32] Avrutsky MI and Troy CM. Caspase-9: a multimodal therapeutic target with diverse cellular expression in human disease. Front Pharmacol 2021; 12: 701301.
[33] Zhou F, Li Y, Huang Y, Wu J, Wu Q, Zhu H and Wang J. Upregulation of CASP9 through NF-kappaB and its target miR-1276 contributed to TNFalpha-promoted apoptosis of cancer cells induced by doxorubicin. Int J Mol Sci 2020; 21: 2290.
[34] Han C, Liu Z, Zhang Y, Shen A, Dong C, Zhang A, Moore C, Ren Z, Lu C, Cao X, Zhang CL, Qiao J and Fu YX. Tumor cells suppress radiation-induced immunity by hijacking caspase 9 signaling. Nat Immunol 2020; 21: 546-554.
[35] Rossi JF, Lu ZY, Jourdan M and Klein B. Interleukin-6 as a therapeutic target. Clin Cancer Res 2015; 21: 1248-1257.
[36] Chavarria-Smith J and Vance RE. The NLRP1 inflammasomes. Immunol Rev 2015; 265: 22-34.
[37] Wang L, Sharif H, Vora SM, Zheng Y and Wu H. Structures and functions of the inflammasome engine. J Allergy Clin Immunol 2021; 147: 2021-2029.
[38] Chen DS and Mellman I. Elements of cancer immunity and the cancer-immune set point. Nature 2017; 541: 321-330.
[39] Yang F, Bettadapura SN, Smeltzer MS, Zhu H and Wang S. Pyroptosis and pyroptosis-inducing cancer drugs. Acta Pharmacol Sin 2022.